Available online at www.sciencedirect.com
SCIENCE DIRECT®
Biochemical and Biophysical Research Communications 324 (2004) 401–408
BBRC
www.elsevier.com/locate/ybbrc

The biochemical activation of T-type Ca^{2+} channels in HEK293 cells stably expressing α_{1G} and Kir2.1 subunits

Taehyun Kim[a], Juhyun Choi[a], Sunoh Kim[a], Ohyeun Kwon[a], Seung-Yeol Nah[b], Ye Sun Han[c,*,1], Hyewhon Rhim[a,*,1]

[a] *Biomedical Research Center, Korea Institute of Science and Technology (KIST), Seoul 136-791, Republic of Korea*
[b] *Department of Physiology, College of Veterinary Medicine, Konkuk University, Seoul 143-701, Republic of Korea*
[c] *Department of Advanced Fusion Technology, Konkuk University, Seoul 143-701, Republic of Korea*

Received 10 September 2004
Available online 25 September 2004

Abstract

In order to investigate the currently unknown cellular signaling pathways of T-type Ca^{2+} channels, we decided to construct a new cell line which would stably express α_{1G} and Kir2.1 subunits in HEK293 cells (HEK293/α_{1G}/Kir2.1). Compared to cells which only expressed α_{1G} (HEK293/α_{1G}), HEK293/α_{1G}/Kir2.1 cells produced an enormous inward rectifying current which was blocked by external Ba^{2+} and Cs^{+} in a concentration-dependent manner. The expression of Kir2.1 channels contributed significantly to the shift of membrane potential from -12.2 ± 2.8 to -57.3 ± 3.7 mV. However, biophysical and pharmacological properties of α_{1G}-mediated Ca^{2+} channels remained unaffected by the expression of Kir2.1 subunits, except for the enlarging of the window current region. Biochemical activation of α_{1G} channels using 150 mM KCl brought about an increase in $[Ca^{2+}]_i$, which was blocked by mibefradil, the T-type Ca^{2+} channel blocker. These data suggest that the HEK293/α_{1G}/Kir2.1 cell line would have potential uses in the study of T-type Ca^{2+} channel-mediated signaling pathways and possibly useful in the development of new therapeutic drugs associated with T-type Ca^{2+} channels.

Keywords: α_{1G} T-type Ca^{2+} channel; Kir2.1; HEK293; Mibefradil; Intracellular Ca^{2+}; Patch-clamp

Voltage-dependent Ca^{2+}channels (VDCCs) induce the entrance of Ca^{2+} into cells along with membrane depolarization. This thereby triggers myriad intracellular events such as contraction, plasticity, secretion, synaptic transmission, and gene expression [1–3]. VDCCs are divided into two main groups on the basis of a voltage requirement for the opening of channels: high-voltage-activated (HVA) and low-voltage-activated (LVA) Ca^{2+} channels. Currently, HVA Ca^{2+} channels are further divided into L-, N-, P/Q-, and R-types, and these functional diversities are related to the existence of several α_1 subunits (α_{1A-F} and α_{1S}). LVA Ca^{2+} channels are easily distinguished from HVA Ca^{2+} channels because they are activated at a potential at a level close to the resting membrane potential. They are referred to as "T-type Ca^{2+} channels" due to their potential for fast inactivation and small conductance [4]. Until recently, three genes which encode T-type Ca^{2+} channel pore-forming subunits had been identified. These were designated $Ca_v3.1$ (α_{1G}), $Ca_v3.2$ (α_{1H}), and $Ca_v3.3$ (α_{1I}) [5–7]. T-type Ca^{2+} channels have been involved in various physiological functions, including cardiac rhythm, smooth muscle contraction, hormone secretion, fertilization, and neuronal firing [4,8–11]. More specifically, neuronal T-type Ca^{2+} channels generate low-threshold spikes that lead to burst firing and rhythmic oscillation [4,12,13].

* Corresponding authors. Fax: +82 2 958 5909 (H. Rhim).
E-mail address: hrhim@kist.re.kr (H. Rhim).
[1] These co-corresponding authors equally contributed to this work.

0006-291X/$ - see front matter © 2004 Elsevier Inc. All rights reserved.
doi:10.1016/j.bbrc.2004.09.069

There are a wide variety of cellular processes which depend on Ca^{2+} influx through VDCCs. An understanding of the mechanisms involved in Ca^{2+}-mediated signal pathways via VDCCs is therefore of crucial importance. The mechanisms involved in T-type Ca^{2+} channel-mediated signal transduction pathways in particular are not well understood. This is mainly attributed to the fast inactivation and small conductance which are characteristic of T-type Ca^{2+} channels [4,8]. Potassium chloride (KCl)-induced depolarization has been frequently used to study the mechanism of the HVA Ca^{2+} channel-mediated signal transduction pathways [14–17]. However, when examined in native neuronal cells, KCl-induced activation of T-type Ca^{2+} channels has caused interference in the greater conductance of HVA Ca^{2+} channels. An additional characteristic of T-type Ca^{2+} channels is that for activation, it requires a membrane potential close to the resting membrane potential. In most heterogeneous expression systems, however, resting membrane potentials are unstably ranged due to the deficiency of endogenous ion channels [18]. Therefore, it has proven quite difficult to activate T-type Ca^{2+} channels using biochemical tools.

To investigate the unknown cellular signaling pathways of T-type Ca^{2+} channels, it is necessary that a useful cell line be found which has a stable resting membrane potential and can activate T-type Ca^{2+} channels with biochemical tools, such as KCl or channel activators. The large, inwardly rectifying family of potassium channel subunits (Kir) consists of seven families, each of which are composed of several members [19–21]. Among them, Kir2 family members show especially strong rectification, which preferentially pass potassium ions into the cell and are involved in the stabilization of the resting membrane potential. It has been demonstrated that Kir2.1 is one of the major determinants involved in resting membrane potential in many cell types [22]. We, therefore, devised human embryonic kidney (HEK293) cells stably transfected with the Kir2.1 subunit (HEK293/α_{1G}/Kir2.1) from the cell's stably expressed α_{1G} subunit, a subset of T-type α_1 subunits (HEK293/α_{1G}), and characterized by the biophysical and pharmacological properties of HEK293/α_{1G}/Kir2.1 cells, as well as by responsiveness to KCl.

Materials and methods

Cloning of human Kir2.1 cDNA. The full-length gene for human Kir2.1 cDNA was amplified from a human brain cDNA library in the plasmid (Takara, Kyoto) with cKir2.1 up (5′-CCGCTCGAGGCCG CCATGGGCAGTGTGAG-3′) and cKir2.1 down (5′-CCGGAATTG TCATATCTCCGATTCTCGCC-3′) used as primers. The PCR product was cloned into the *Xho*I/*Eco*RI site of pCMVpuro (Clontech).

Generation of Kir2.1 stably transfected cells (HEK293/α_{1G}/Kir2.1). HEK293 cells which stably express the human α_{1G} subunit of T-type Ca^{2+} channels (HEK293/α_{1G}) were kindly provided from Dr. Perez-Reyes (University of Virginia) and grown in Dulbecco's modified Eagle's medium (DMEM), which contained 10% fetal bovine serum, penicillin (100 U/ml), streptomycin (100 μg/ml), and geneticin (500 μg/ml). For the HEK293/α_{1G}/Kir2.1 cell line, Kir2.1 (cloned into pCMVpuro) was transfected with HEK293/α_{1G} cells using pEQPAM3 and pVSV-G (Clontech) in order to produce a retrovirus which would include the Kir2.1 gene. These retrovirus-infected HEK293/α_{1G} cells were positively selected with puromycin (1 μg/ml) in DMEM for with the purpose of generating a HEK293/α_{1G}/Kir2.1 cell line which stably expressed both α_{1G} and Kir2.1 subunits. Cells were incubated in a humid atmosphere of 5% CO_2 and 95% air at 37 °C.

Reverse Transcription PCR (RT-PCR). Total RNA of HEK293/α_{1G} or HEK293/α_{1G}/Kir2.1 cells was isolated with easy-BLUE reagent (iNtRON, Korea) in accordance with the manufacturer's instructions. First-strand cDNA was generated from total RNA using PowerScript reverse transcriptase (Clontech). The sequences of sense and antisense primers for the Kir2.1 gene fragment are as follows: sense: 5′-AG GTCAACAGCTTACCGGCTG-3′, antisense: 5′-CACCATGCCTT CCAGTATCAC-3′. The expected Kir2.1 gene fragment length which resulted from cDNA amplification is 522 bp. β-Actin gene was used for positive amplification control. The primers for β-actin which resulted in cDNA fragments of 510 bp had the following sequences: sense: 5′-G TCACCAACTGGGACGACATG-3′, antisense: 5′-GCCGTCAGGC AGCTCGTAGC -3′. In order to cause the amplification of the specific fragments of Kir2.1 or β-actin, the PCR was performed with Takara Ex Taq (Takara Shuzo, Japan). The cycle conditions were: initial denaturation at 50 °C for 30 min and 94 °C for 2 min, which was followed by 35 amplification cycles at 94 °C for 30 s, annealing at 50 °C for 30 s, and elongation at 72 °C for 1 min. The PCR products were resolved in 1% agarose gel with ethidium bromide.

Western blot analysis. Cells were rinsed twice for 20 min at 4 °C with ice-cold phosphate-buffered saline (PBS) and subsequently lysed with 50 mM Hepes buffer (pH 7.5) which contained 150 mM NaCl, 10% glycerol, 1% Triton X-100, 1.5 mM $MgCl_2$, 1 mM EGTA, 10 μg/ml leupeptin, 10 μg/ml aprotinin, 1 mM phenylmethylsulfonyl fluoride, and 0.2 mM sodium orthovanadate. The cells were then scraped from dishes and centrifuged at 15,000*g* for 20 min at 4 °C. The lysates were further denatured for 5 min at 95 °C in a sample buffer solution (2% SDS, 10% glycerol, 60 mM Tris (pH 6.8), 5% β-mercaptoethanol, and 0.01% bromphenol blue). Protein samples were then resolved on a 10% polyacrylamide SDS gel and transferred to a polyvinylidene difluoride membrane (Millipore). The membranes were blocked in Tris-buffered saline (TBS; 20 mM Tris–Cl, pH 7.6, 137 mM NaCl) with 5% skim milk. Blots were incubated with the primary antibody (rabbit anti-human Kir2.1 antibody, United States Biological), diluted to 2 μg/ml in TBS + 5% milk for 4 h at room temperature, washed three times in TBS + 0.5% Tween 20, and then incubated for 45 min in horseradish peroxidase-conjugated secondary antibody (1:10,000) (Santa Cruz Biotechnology). Blots were developed using the ECL detection kit (Amersham Biosciences).

Electrophysiological recordings. Electrophysiological recordings were achieved using whole-cell patch-clamp techniques at room temperature. Borosilicate glass electrodes with a resistance of 3–4 MΩ were pulled and coated with Sylgard. For the recording of resting membrane potentials, the nystatin perforated patch-clamp method was employed. Patch electrodes were filled with the internal solution, which contained (in mM): 30 KCl, 90 KOH, 90 L-aspartic acid, 1 $MgCl_2$, 10 NaCl, and 10 Hepes. Nystatin was prepared as a stock solution (25 mg/ml) in DMSO and, using the internal solution, diluted to a concentration of 250 μg/ml and back-filled into the pipette after the tip of the pipette was first filled with the nystatin-free solution. The external solution contained (in mM): 140 NaCl, 3 KCl, 1 $MgCl_2$, 1.5 $CaCl_2$, 10 Hepes, and 10 glucose (pH 7.4). For the recordings of Kir2.1 and T-type Ca^{2+} currents, the standard whole-cell patch-clamp method was utilized. The composition of the internal solution for Kir2.1 currents contained (in mM): 140 K-gluconate, 2 $MgCl_2$, 1

EGTA, 1 Na_2ATP, and 5 Hepes. This external solution contained: 135 NaCl, 5 KCl, 1 $MgCl_2$, 1.8 $CaCl_2$, 5 Hepes, and 10 glucose (pH 7.4). For the recording of T-type Ca^{2+} currents, the composition of the internal solution contained (in mM): 130 KCl, 11 EGTA, 10 Hepes, and 5 Mg-ATP (pH 7.4), and the external solution contained: 140 NaCl, 2 $CaCl_2$, 10 glucose, and 10 Hepes (pH 7.4). The current recordings were obtained using an EPC-9 amplifier and Pulse/Pulsefit software program (HEKA, Germany).

Intracellular Ca^{2+} imaging. The acetoxymethyl-ester form of fura-2 (fura-2/AM; Molecular probes, Eugene, OR) was applied as the fluorescent Ca^{2+} indicator. The cells were then incubated for 60 min at room temperature with 5 μM fura-2/AM and 0.001% Pluronic F-127 in a Hepes-buffered solution, the composition of which was (in mM): 150 NaCl, 5 KCl, 1 $MgCl_2$, 2 $CaCl_2$, 10 Hepes, and 10 glucose (pH 7.4). After they were washed, cells were illuminated with a xenon arc lamp. The required excitation wavelengths (340 and 380 nm) were selected by a computer-controlled filter wheel (Sutter Instruments, CA). Data were acquired every 2 s and a shutter between exposures in the light path was interposed in order to protect the cells from phototoxicity. Emitter fluorescence was reflected through a 515 nm long-pass filter to a frame transfer cooled CCD camera. The ratios of emitted fluorescence were then calculated using a digital fluorescence analyzer and subsequently converted to an intracellular Ca^{2+}concentration ($[Ca^{2+}]_i$). All imaging data were collected and analyzed using Universal Imaging software (West Chester, PA).

Data analysis. Data were analyzed using Pulse/Pulsefit (HEKA, Germany) and GraphPad Prism (GraphPad) software programs. Whole cell current-voltage (*I–V*) curves of Ca^{2+} currents were fitted using the following modified Boltzmann equation:

$$I = G_{max}(V - V_{rev})/(1 + \exp(-(V - V_{0.5})/k)),$$

where G_{max} represents maximum conductance, V_{rev} represents the reversal potential, and $V_{0.5}$ represents the potential of half-maximal current activation. The slope factor is represented by k. The curves for steady-state activation (m_∞) and inactivation (h_∞) were then fitted using a Boltzmann equation:

$$I = I_{min} + (I_{max} - I_{min})/(1 + \exp((V_{0.5} - V)/k)),$$

where I_{min} and I_{max} are normalized minimum and maximum currents, respectively.

All results are presented as means ± SE, where n denotes the number of cells examined. The significance of observed differences was evaluated using Student's unpaired t test.

Results and discussion

RT-PCR and Western blot analysis of Kir2.1 subunit in stably transfected cells

The stable expression of the Kir2.1 subunit was explored in HEK293 cells with RT-PCR. RT-PCR analysis of total RNA isolated from Kir2.1-transfected (HEK293/α_{1G}/Kir2.1) and untransfected control (HEK293/α_{1G}) cells is shown in Fig. 1A. HEK293/α_{1G}/Kir2.1 cells exhibited the expected PCR product for the Kir2.1 subunit (522 bp). This was observed in all samples from six consecutively cultured passages. This PCR product was not observed in the control cells, which were untransfected.

To confirm a biologically relevant Kir2.1 expression, application of the Western blot analysis of membrane protein was necessary. The antibody directed against

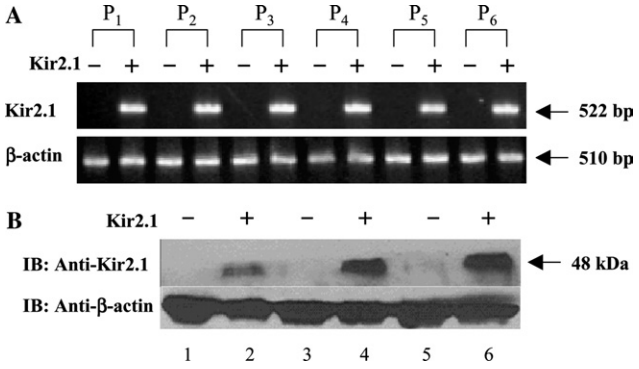

Fig. 1. RT-PCR and Western blot analysis of Kir2.1 subunit in stably transfected cells. (A) Agarose gel electrophoresis of Kir2.1 fragments amplified from cDNA preparations of Kir2.1-transfected (HEK293/α_{1G}/Kir2.1; +) and control (HEK293/α_{1G}; −) cells. HEK293/α_{1G}/Kir2.1 cells exhibited the expected PCR product for the Kir2.1 subunit (522 bp). This PCR product was not observed in untransfected control cells. When the β-actin gene was used for positive amplification control, the expected PCR product for β-actin (510 bp) was detected in both cell lines. (B) Western blot detection of Kir2.1 protein. Cell lysates (35 μg) prepared from HEK293/α_{1G}/Kir2.1 (+) and HEK293/α_{1G} (−) cells were resolved by SDS–polyacrylamide gel electrophoresis (10% polyacrylamide) and transferred to a polyvinylidene difluoride membrane. An antibody specific to human Kir2.1 was used for Western blot analysis (top panel). Protein loading efficiency was normalized by β-actin (bottom panel). To verify the stable expression of Kir2.1 in HEK293/α_{1G}/Kir2.1 cells, the experiment was repeated with cells obtained from six (P_1–P_6) and three consecutively cultured passages for RT-PCR and Western blot analysis, respectively.

human Kir2.1 was used in order to probe for Kir2.1 protein. As shown in Fig. 1B, Kir2.1 is substantially expressed as a 48 kDa protein in Kir2.1-transfected HEK293/α_{1G}/Kir2.1 cells (Fig. 1B, upper panel, lanes 2, 4, and 6). No bands were detected by anti-human Kir2.1 antibody in the control HEK293/α_{1G} cells (lanes 1, 3, and 5). The membrane was probed with an antibody for β-actin to demonstrate that loading efficiency was consistent in all lanes (Fig. 1B, bottom panel). Altogether, these results provide verification that the Kir2.1 subunit is stably expressed in HEK293/α_{1G}/Kir2.1 cells.

Functional analysis of Kir2.1 channels using electrophysiological recordings

For confirmation of the functional expression of Kir2.1 subunits, we directly measured inward rectifying potassium currents using whole-cell patch-clamp recordings. Whole-cell currents were acquired for 200 ms depolarizing pulses from −140 to −40 mV (holding potential of −60 mV) with 10 mV voltage increments. Figs. 2A and B show mean steady state current–voltage (*I–V*) relations recorded in HEK293/α_{1G} and HEK293/α_{1G}/Kir2.1 cells, respectively. In comparison to HEK293/α_{1G} cells, HEK293/α_{1G}/Kir2.1 cells produced a massive inward current with a strong rectification. The expression of Kir2.1 subunits significantly increased the inward rectifying currents from −120.0 ± 26.5 to

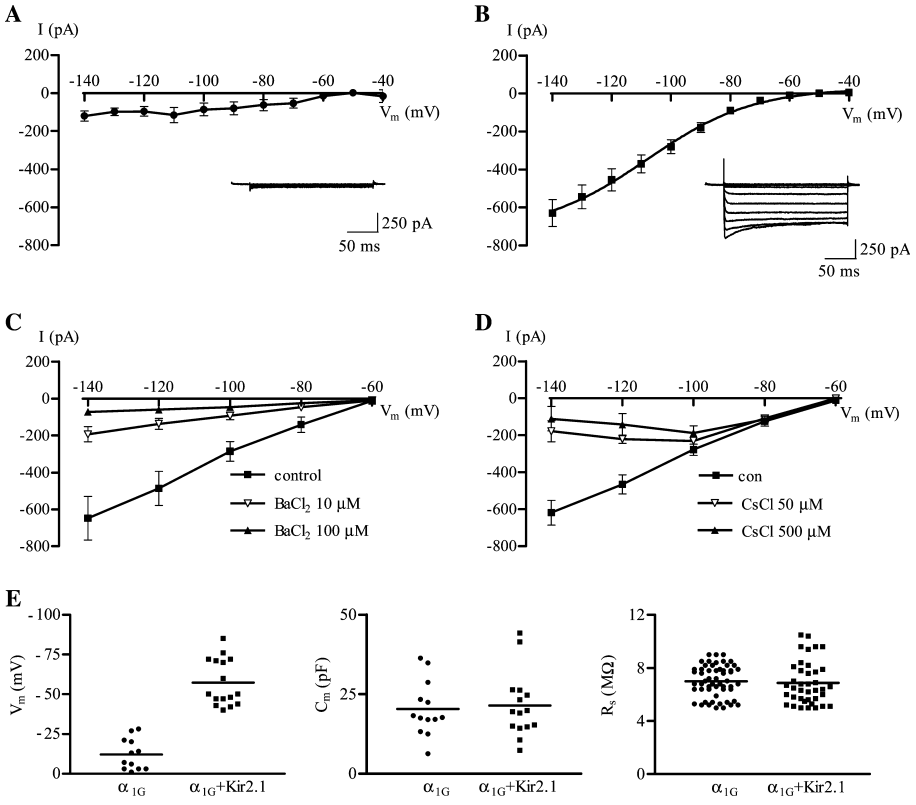

Fig. 2. Electrophysiological properties of inward rectifying potassium currents in HEK293/α_{1G}/Kir2.1 cells. (A,B) Mean steady-state current–voltage (*I–V*) relationships in HEK293/α_{1G} cells (●, $n = 8$) and HEK293/α_{1G}/Kir2.1 cells (■, $n = 11$), respectively. Whole-cell inward currents were evoked in response to a 200 ms voltage step from −140 mV to −40 mV in 10 mV increments from a holding potential of −60 mV. Representative traces of whole-cell currents obtained from each evoked potential are shown in the inset. Steady-state *I–V* relationships of whole-cell currents were recorded with varying extracellular concentrations of Ba^+ (C) and Cs^+ (D). Whole-cell currents were evoked using the same protocol as in (A), except the increments were 20 mV rather than 10 mV. (E) Comparison of resting membrane potential (V_m), cell capacitance (C_m), and series resistance (R_s) between two cell lines.

-629.7 ± 71.3 at -140 mV ($P < 0.001$, $n = 8$–11). Besides the increased inward rectifying current, HEK293/α_{1G}/Kir2.1 cells also showed another characteristic feature of Kir channels: a blockade created by external cations like Ba^{2+} and Cs^+. Kir currents were inhibited by external Ba^{2+} and Cs^+ in a concentration- and voltage-dependent manner (Figs. 2C and D). If Kir2.1 currents are, in fact, responsible for the increased inward currents as described above, it is likely that they would also be involved in setting the membrane potential of HEK293/α_{1G}/Kir2.1 cells. We therefore examined whether or not Kir2.1 channels would, in fact, contribute to the setting of a new resting membrane potential in HEK293/α_{1G}/Kir2.1 cells. The resting membrane potentials of HEK293/α_{1G}, Kir2.1-untransfected cells, ranged from -28 to 0 mV (-12.2 ± 2.8 mV, $n = 12$). The expression of Kir2.1 channels, however, caused a significant shift in the resting membrane potential to a more hyperpolarized potential ranging from -40 to -85 mV in HEK293/α_{1G}/Kir2.1 cells ($P < 0.001$, -57.3 ± 3.7 mV, $n = 16$). No significant differences existed in relation to the cell capacitance (C_m) and the series resistance (R_s) between the two cell lines (Fig. 2E).

Effect of Kir2.1 subunit expression on biophysical and pharmacological properties of α_{1G} T-type Ca^{2+} channels

We next examined whether the expression of Kir 2.1 subunits has an effect on the biophysical and pharmacological properties of α_{1G} T-type Ca^{2+} channels. T-type Ca^{2+} channels, including recombinant three Ca_v3 clones, characteristically begin to activate at about -60 mV and typically produce a maximum current around -30 mV at the *I–V* curves [4,23,24]. Figs. 3A and B illustrate mean *I–V* curves of α_{1G} T-type Ca^{2+} channels in HEK293/α_{1G} and HEK293/α_{1G}/Kir2.1 cells, respectively. Both HEK293/α_{1G} and HEK293/α_{1G}/Kir2.1 cells began activation at about -60 mV and produced a maximum current around -30 mV. There was no significant difference in relation to the peak current amplitudes measured at -30 mV from the holding potential of -100 mV (495.3 ± 53.1 for HEK293/α_{1G} and 528.4 ± 65.2 pA for HEK293/α_{1G}/Kir2.1 cells, $n = 9$). The detailed biophysical parameters of α_{1G} T-type Ca^{2+} channels were investigated by examining the steady-state activation and deactivation properties. Steady-state activation of the α_{1G} channel was determined after

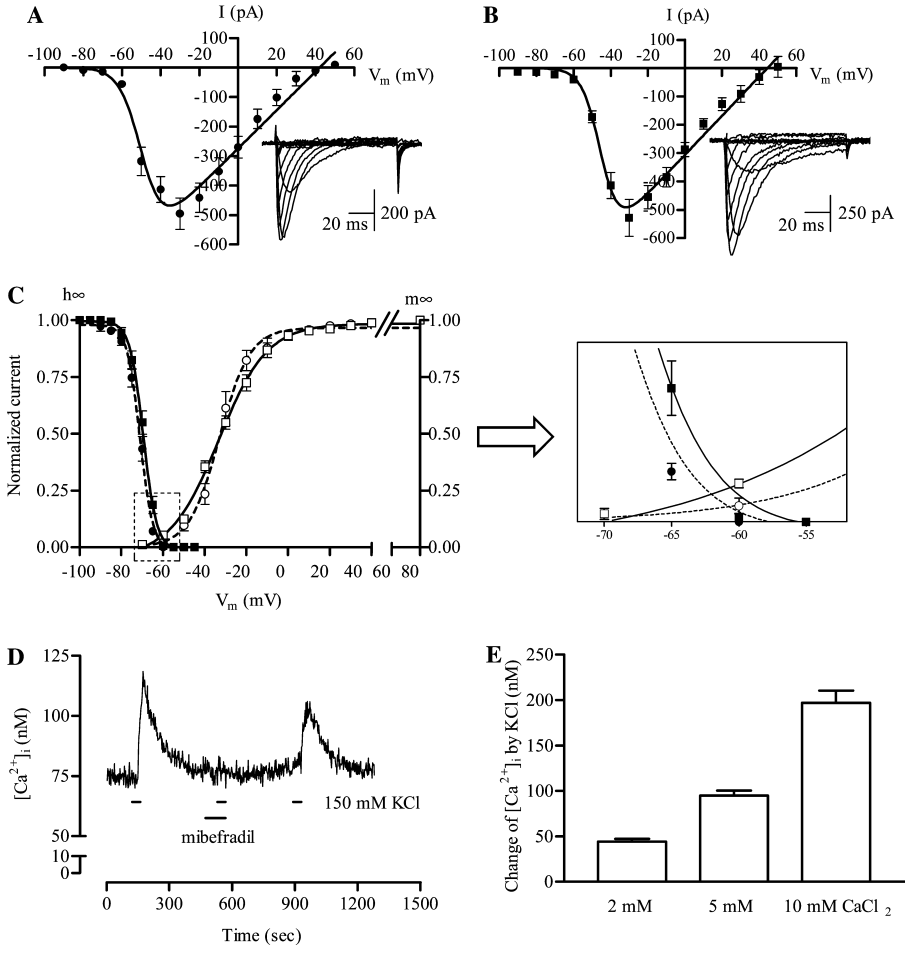

Fig. 3. Electrophysiological properties of α_{1G} Ca^{2+} channels and high KCl-mediated $[Ca^{2+}]_i$ increase in HEK293/α_{1G}/Kir2.1 cells. (A,B) Mean peak Ca^{2+} current-voltage (I–V) relationships in HEK293/α_{1G} (●, $n = 9$) and HEK293/α_{1G}/Kir2.1 cells (■, $n = 9$), respectively. Whole-cell Ca^{2+} currents were evoked from the holding potential of −100 mV with 100 ms depolarizing pulses (−90 mV to 50 mV, 10 mV-increment). Representative traces of whole-cell Ca^{2+} currents obtained from each evoke potential are shown in the inset. (C) Steady-state activation and inactivation of α_{1G} Ca^{2+} currents. Steady-state activation was determined by measuring tail current amplitudes at various depolarizing pulses. For each depolarization, the tail current amplitude was measured for pulse durations adjusted from the membrane potential/time-to-peak plot as previously described [26]. Steady-state inactivation was determined from the measurement of the current amplitude at −30 mV after a pre-depolarization pulse (5 s) of increasing amplitude (−100 to −45 mV, 5 mV-increment). Mean steady-state activation (open) and inactivation (filled symbols) curves of HEK293/α_{1G} (circle symbols with dotted line) and HEK293/α_{1G}/Kir2.1 (square symbols with solid line) cells were fitted by a Boltzmann equation. The arrowed box shows the enlarged window current, obtained via the overlap in the steady-state activation (m_∞) and inactivation (h_∞) curves, near −72 to −52 mV. (D) Measurement of $[Ca^{2+}]_i$ in HEK293/α_{1G}/Kir2.1 cells. Application of 150 mM KCl (30 s) produced a transient increase of $[Ca^{2+}]_i$, which was blocked by co-treatment of mibefradil (10 μM, 1 min), the potent T-type Ca^{2+}channel blocker. The Hepes-buffered solution with 150 mM KCl was made by replacing an equivalent amount of NaCl. (E) 150 mM KCl-induced change of $[Ca^{2+}]_i$ in the presence of 2, 5, and 10 mM $CaCl_2$ in HEK293/α_{1G}/Kir2.1 cells.

measuring tail current amplitudes at various depolarizing pulses and fitted by a Boltzmann equation (described in Materials and methods). Mean potentials for half-activation ($V_{0.5\ -\ act}$) were insignificantly different: -32.9 ± 0.8 mV for HEK293/α_{1G} ($n = 9$) and -33.4 ± 0.8 mV for HEK293/α_{1G}/Kir2.1 ($n = 14$). However, the values for slope activation factor (k_{act}) proved significantly different (7.3 ± 0.7 and 11.7 ± 0.7, $P < 0.001$). Steady-state inactivation properties were determined from the measurement of the current amplitude at −30 mV after a pre-depolarization pulse of increasing amplitude. The mean potential of half-inactivation ($V_{0.5\ -\ inact}$) was shifted from -71.1 ± 0.3 mV for HEK293/α_{1G} to -69.5 ± 0.2 mV for HEK293/α_{1G}/Kir2.1 with no apparent changes in slope inactivation factor (k_{inact} 3.1 ± 0.3 and -3.2 ± 0.2). The difference in $V_{0.5\ -\ inact}$ was small, but still statistically significant ($P < 0.01$, $n = 5$). As a consequence of changes in steady-state activation and inactivation properties, a window current region obtained by superimposed steady-state activation (m_∞) and inactivation (h_∞) curves was enlarged by the expression of Kir2.1 channels (Fig. 3C). Therefore, HEK293/α_{1G}/Kir2.1 cells can generate a window current at membrane potentials in the range

of −70/55 mV, which is very close to the resting membrane potential of this newly devised cell line (−57.3 ± 3.7 mV). These results suggest that α_{1G} T-type Ca^{2+} channels may activate and regulate Ca^{2+} signaling at resting membrane potential in HEK293/α_{1G}/Kir2.1 cells.

It is well known that human α_{1G} channels are quite sensitive to two molecules, nickel (Ni^{2+}) and mibefradil, both of which are regarded to be T-type channel blockers. We, therefore, compared the IC_{50} of these two channel blockers in HEK293/α_{1G} and HEK293/α_{1G}/Kir2.1 cells. The divalent ion Ni^{2+} block of human α_{1G} channels was modest, with an IC_{50} of 83.7 and 109.0 μM in HEK293/α_{1G} and HEK293/α_{1G}/Kir2.1 cells, respectively. However, mibefradil, the most potent T-type channel blocker, inhibited α_{1G} current amplitude with an IC_{50} of 0.92 and 0.51 μM in HEK293/α_{1G} and HEK293/α_{1G}/Kir2.1 cells, respectively. These results are consistent with those of previous studies on recombinant T-type channels [25,26] and suggest that the expression of Kir2.1 channels causes no pharmacological changes to α_{1G} T-type Ca^{2+} channel properties. The biophysical and pharmacological properties of HEK293/α_{1G} and HEK293/α_{1G}/Kir2.1 cells are summarized in Table 1.

High KCl-mediated $[Ca^{2+}]_i$ increase in HEK293/α_{1G}/Kir2.1 cells

The goal of the present study was to create a useful cell line which can activate T-type Ca^{2+} channels by KCl-mediated depolarization. The preceding results of this study suggest that α_{1G} T-type Ca^{2+} channels can activate and regulate Ca^{2+} signaling at resting membrane potential levels in HEK293/α_{1G}/Kir2.1 cells. To confirm the activation of α_{1G} T-type Ca^{2+} channels using KCl at resting membrane potential, KCl-mediated changes were measured in intracellular Ca^{2+}concentration ($[Ca^{2+}]_i$) utilizing fura-2 based digital imaging techniques. In HEK293/α_{1G} cells, change of $[Ca^{2+}]_i$ by 150 mM treatment of KCl was undetectable (data not shown). However, application of high concentration KCl (70 or 150 mM, 30 s) produced a transient increase of $[Ca^{2+}]_i$ in HEK293/α_{1G}/Kir2.1 cells. Treatment of 150 mM KCl stimulated the increase of $[Ca^{2+}]_i$ from 75 to 120 nM in a regular Hepes-buffered solution (Fig. 3D). The Hepes-buffered solution with 70 or 150 mM KCl was made by replacing an equivalent amount of NaCl. Furthermore, this increase was totally blocked by co-treatment with 10 μM mibefradil, the most potent T-type Ca^{2+}channel blocker, with partial recovery. Because the long treatment of high concentrations of KCl can prove detrimental to cell homeostasis, we examined whether the signal of $[Ca^{2+}]_i$ could be amplified by extracellular concentration of $CaCl_2$. Fig. 3E shows the KCl-mediated change of $[Ca^{2+}]_i$ caused by varied concentrations of extracellular $CaCl_2$. The increments of $[Ca^{2+}]_i$ change were consistent with increasing concentrations of $CaCl_2$: 44.1 ± 3.3 for 2 mM, 94.8 ± 5.6 for 5 mM, and 196.8 ± 13.8 nM for 10 mM $CaCl_2$ ($n = 15$). It leaves the possibility of varying concentrations of KCl and $CaCl_2$ dependent on the protocol in relation to T-type Ca^{2+} channel activation. These results indicate that the increase in $[Ca^{2+}]_i$ by KCl-induced depolarization is fully responsible for α_{1G} channel activation in HEK293/α_{1G}/Kir2.1 cells. Altogether, the detailed functional analysis performed in this study by comparing HEK293/α_{1G} and HEK293/α_{1G}/Kir2.1 cells provides compelling evidence that the stable expression of Kir2.1 channels only made it possible to construct a cell line capable of activating T-type Ca^{2+} channels by KCl-mediated depolarization. The expression of Kir2.1 channels increased a superimposed area of steady-state activation and inactivation curves, as well as caused a shift in resting membrane potential from −12.2 ± 2.8 to −57.3 ± 3.7 mV. Finally, this made it possible to activate human α_{1G} channels through the use of biochemical tools such as KCl or T-type channel activators.

The specific features described here for the construction of HEK293/α_{1G}/Kir2.1 cells should be useful in identifying unknown cellular signaling pathways of T-type Ca^{2+} channels. Recently, the mechanisms of cellular signaling pathways of HVA VDCCs along with membrane depolarization have been intensively studied. It has been reported that mitogen-activated protein (MAP) kinase could play an important role in linking

Table 1
Summary of electrophysiological and pharmacological properties in HEK293/α_{1G} and HEK293/α_{1G}/Kir2.1 cells

	HEK293/α_{1G}	HEK293/α_{1G}/Kir2.1
Resting membrane potential (mV)	−12.2 ± 2.8	−57.3 ± 3.7***
$I_{amplitude}$ (pA)		
I_{Kir} at −140 mV	−120.0 ± 26.5	−629.7 ± 71.3***
I_{Ca} at −30 mV	−495.3 ± 53.1	−528.4 ± 65.2
Steady-state activation		
$V_{0.5-act}$ (mV)	−32.9 ± 0.8	−33.4 ± 0.8
Slope (k_{act})	7.3 ± 0.7	11.7 ± 0.7***
Steady-state inactivation		
$V_{0.5-inact}$ (mV)	−71.1 ± 0.3	−69.5 ± 0.2**
Slope (k_{act})	−3.1 ± 0.3	−3.2 ± 0.2
IC_{50} values of		
Ni^{2+} (μV)	83.7	109.0
Mibefradil (μM)	0.92	0.51

The statistical significance of the differences between two cell lines was estimated using a Student's unpaired t test. The IC_{50}values of Ni^{2+} and mibefradil were obtained from computer fit of mean values to the three-parameter logistic equation, $I = I_{min} + (I_{max} - I_{min})/(1 + 10^{(Log\ IC_{50} - X)})$, where I denotes inhibition of Ca^{2+} currents in the presence of blocker, I_{min} and I_{max} are the minimum and maximum inhibition, respectively, and X is the logarithm of blocker.

membrane depolarization to gene expression in postsynaptic neurons [1,27]. Ca^{2+} influx through L-type Ca^{2+} channels is particularly effective in activating transcription factors such as CREB and MEF-2 [28,29]. In detail, a complex between the Ca^{2+} binding protein, calmodulin, and an L-type Ca^{2+} channel is necessitated to trigger the Ras/mitogen-activated protein kinase (MAPK) pathway [30]. Hibino et al. [31] showed that RIM binding proteins (RBPs) interact with α_{1D} (L-type) and α_{1B} (N-type) Ca^{2+} channel subunits in various cells. For P/Q-type Ca^{2+} channels, Tomizawa et al. [32] have shown that the complex of cyclin-dependent kinase 5 (Cdk5) and p35, the neuron-specific regulatory subunit of Cdk5, inhibits neurotransmitter release through the phosphorylation and downregulation of P/Q-type Ca^{2+} channels. Compared to these studies of HVA VDCCs, the mechanisms involved in T-type Ca^{2+} channel-mediated signal transduction pathways are not well understood. Using this valuable cell line, we are currently investigating the signal transduction pathways of α_{1G} T-type Ca^{2+} channels after activation by KCl treatment. We have found that α_{1G} activation actually reduced the activation of $p21^{ras}$ with correlated ERK activity, as well as with other downstream signaling molecules of $p21^{ras}$ (manuscript in preparation).

Another appeal is the possible application of HEK293/α_{1G}/Kir2.1 cells for the development of selective T-type Ca^{2+} channel blockers. Many studies have suggested the possibility of T-type Ca^{2+} channel blockers as drug targets due to their implications in the pathogenesis of epilepsy and neuropathic pain [4,13,33]. To date, only limited progress has been made in the quest to identify both potent and selective compounds for T-type Ca^{2+} channel blockers. Although mibefradil has been found to potently inhibit T-type Ca^{2+} channels, it is not only targeting other ion channels, but also producing toxicity due to drug–drug interaction [8,34]. The investigation of new T-type Ca^{2+} channel blockers, therefore, is needed to understand the exact role of T-type Ca^{2+} channels and to develop clinically applicable drug targets. Recently, high-throughput screening (HTS) assays are increasingly relied upon to generate early and novel discovery leads for drug development. Designing fluorescence-based HTS assays for ion channel drug discovery has proved to be a tremendous challenge for the pharmaceutical industry. The development of this process would be especially valuable because it could improve the limitation of electrophysiological-based time-consuming assays. Herein, a new cell line (HEK293/α_{1G}/Kir2.1) devised from the present study could be useful for analyzing α_{1G} T-type Ca^{2+} channel-mediated signaling pathways and offer a potential HTS approach to discovering new therapeutic drugs associated with T-type Ca^{2+} channels.

Acknowledgments

This work was supported in part by grants from the Vision 21 Program (KIST), the Brain Research Center of the 21st Century Frontier Research Program (M103KV010004-03K2201-00420), and KRCF Strategic R&D Program, Korea. The authors extend their appreciation to Dr. Perez-Reyes for providing HEK293 cells stably expressing human α_{1G} T-type Ca^{2+} channels.

References

[1] A. Ghosh, M.E. Greenberg, Calcium signaling in neurons: molecular mechanisms and cellular consequences, Science 268 (1995) 239–247.
[2] M.J. Berridge, Neuronal calcium signaling, Neuron 21 (1998) 13–26.
[3] W.A. Catterall, Structure and regulation of voltage-gated Ca2+ channels, Annu. Rev. Cell Dev. Biol. 16 (2000) 521–555.
[4] J.R. Huguenard, Low-threshold calcium currents in central nervous system neurons, Annu. Rev. Physiol. 58 (1996) 329–348.
[5] L.L. Cribbs, J.H. Lee, J. Yang, J. Satin, Y. Zhang, A. Daud, J. Barclay, M.P. Williamson, M. Fox, M. Rees, E. Perez-Reyes, Cloning and characterization of alpha1H from human heart, a member of the T-type Ca2+ channel gene family, Circ. Res. 83 (1998) 103–109.
[6] E. Perez-Reyes, L.L. Cribbs, A. Daud, A.E. Lacerda, J. Barclay, M.P. Williamson, M. Fox, M. Rees, J.H. Lee, Molecular characterization of a neuronal low-voltage-activated T-type calcium channel, Nature 391 (1998) 896–900.
[7] J.H. Lee, A.N. Daud, L.L. Cribbs, A.E. Lacerda, A. Pereverzev, U. Klockner, T. Schneider, E. Perez-Reyes, Cloning and expression of a novel member of the low voltage-activated T-type calcium channel family, J. Neurosci. 19 (1999) 1912–1921.
[8] E. Perez-Reyes, Molecular physiology of low-voltage-activated T-type calcium channels, Physiol. Rev. 83 (2003) 117–161.
[9] Z. Zhou, S.L. Lipsius, T-type calcium current in latent pacemaker cells isolated from cat right atrium, J. Mol. Cell. Cardiol. 26 (1994) 1211–1219.
[10] M.F. Rossier, M.M. Burnay, M.B. Vallotton, A.M. Capponi, Distinct functions of T- and L-type calcium channels during activation of bovine adrenal glomerulosa cells, Endocrinology 137 (1996) 4817–4826.
[11] C. Arnoult, R.A. Cardullo, J.R. Lemos, H.M. Florman, Activation of mouse sperm T-type Ca2+ channels by adhesion to the egg zona pellucida, Proc. Natl. Acad. Sci. USA 93 (1996) 13004–13009.
[12] S.W. Hughes, D.W. Cope, K.L. Blethyn, V. Crunelli, Cellular mechanisms of the slow (<1 Hz) oscillation in thalamocortical neurons in vitro, Neuron 33 (2002) 947–958.
[13] D. Kim, I. Song, S. Keum, T. Lee, M.J. Jeong, S.S. Kim, M.W. McEnery, H.S. Shin, Lack of the burst firing of thalamocortical relay neurons and resistance to absence seizures in mice lacking alpha(1G) T-type Ca(2+) channels, Neuron 31 (2001) 35–45.
[14] J. Robidoux, L. Simoneau, A. Masse, J. Lafond, Activation of L-type calcium channels induces corticotropin-releasing factor secretion from human placental trophoblasts, J. Clin. Endocrinol. Metab. 85 (2000) 3356–3364.
[15] M. Kansha, T. Nagata, K. Irita, S. Takahashi, Dibucaine and tetracaine inhibit the activation of mitogen-activated protein kinase mediated by L-type calcium channels in PC12 cells, Anesthesiology 91 (1999) 1798–1806.

[16] E. Gomez, C. Pritchard, T.P. Herbert, cAMP-dependent protein kinase and Ca2+ influx through L-type voltage-gated calcium channels mediate Raf-independent activation of extracellular regulated kinase in response to glucagon-like peptide-1 in pancreatic beta-cells, J. Biol. Chem. 277 (2002) 48146–48151.
[17] W. Macias, R. Carlson, A. Rajadhyaksha, A. Barczak, C. Konradi, Potassium chloride depolarization mediates CREB phosphorylation in striatal neurons in an NMDA receptor-dependent manner, Brain Res. 890 (2001) 222–232.
[18] S.P. Yu, G.A. Kerchner, Endogenous voltage-gated potassium channels in human embryonic kidney (HEK293) cells, J. Neurosci. Res. 52 (1998) 612–617.
[19] C.G. Nichols, A.N. Lopatin, Inward rectifier potassium channels, Annu. Rev. Physiol. 59 (1997) 171–191.
[20] D. Bichet, F.A. Haass, L.Y. Jan, Merging functional studies with structures of inward-rectifier K(+) channels, Nat. Rev. Neurosci. 4 (2003) 957–967.
[21] N. Takahashi, K. Morishige, A. Jahangir, M. Yamada, I. Findlay, H. Koyama, Y. Kurachi, Molecular cloning and functional expression of cDNA encoding a second class of inward rectifier potassium channels in the mouse brain, J. Biol. Chem. 269 (1994) 23274–23279.
[22] H.J. Jongsma, R. Wilders, Channelopathies: Kir2.1 mutations jeopardize many cell functions, Curr. Biol. 11 (2001) R747–750.
[23] U. Klockner, J.H. Lee, L.L. Cribbs, A. Daud, J. Hescheler, A. Pereverzev, E. Perez-Reyes, T. Schneider, Comparison of the Ca2+ currents induced by expression of three cloned alpha1 subunits, alpha1G, alpha1H and alpha1I, of low-voltage-activated T-type Ca2+ channels, Eur. J. Neurosci. 11 (1999) 4171–4178.
[24] E. Carbone, H.D. Lux, A low voltage-activated calcium conductance in embryonic chick sensory neurons, Biophys. J. 46 (1984) 413–418.
[25] A. Monteil, J. Chemin, V. Leuranguer, C. Altier, G. Mennessier, E. Bourinet, P. Lory, J. Nargeot, Specific properties of T-type calcium channels generated by the human alpha 1I subunit, J. Biol. Chem. 275 (2000) 16530–16535.
[26] A. Monteil, J. Chemin, E. Bourinet, G. Mennessier, P. Lory, J. Nargeot, Molecular and functional properties of the human alpha(1G) subunit that forms T-type calcium channels, J. Biol. Chem. 275 (2000) 6090–6100.
[27] S. Finkbeiner, M.E. Greenberg, Ca(2+)-dependent routes to Ras: mechanisms for neuronal survival, differentiation, and plasticity?, Neuron 16 (1996) 233–236.
[28] S. Finkbeiner, S.F. Tavazoie, A. Maloratsky, K.M. Jacobs, K.M. Harris, M.E. Greenberg, CREB: a major mediator of neuronal neurotrophin responses, Neuron 19 (1997) 1031–1047.
[29] Z. Mao, A. Bonni, F. Xia, M. Nadal-Vicens, M.E. Greenberg, Neuronal activity-dependent cell survival mediated by transcription factor MEF2, Science 286 (1999) 785–790.
[30] R.E. Dolmetsch, U. Pajvani, K. Fife, J.M. Spotts, M.E. Greenberg, Signaling to the nucleus by an L-type calcium channel-calmodulin complex through the MAP kinase pathway, Science 294 (2001) 333–339.
[31] H. Hibino, R. Pironkova, O. Onwumere, M. Vologodskaia, A.J. Hudspeth, F. Lesage, RIM binding proteins (RBPs) couple Rab3-interacting molecules (RIMs) to voltage-gated Ca(2+) channels, Neuron 34 (2002) 411–423.
[32] K. Tomizawa, J. Ohta, M. Matsushita, A. Moriwaki, S.T. Li, K. Takei, H. Matsui, Cdk5/p35 regulates neurotransmitter release through phosphorylation and downregulation of P/Q-type voltage-dependent calcium channel activity, J. Neurosci. 22 (2002) 2590–2597.
[33] A. Dogrul, L.R. Gardell, M.H. Ossipov, F.C. Tulunay, J. Lai, F. Porreca, Reversal of experimental neuropathic pain by T-type calcium channel blockers, Pain 105 (2003) 159–168.
[34] J.C. Krayenbuhl, S. Vozeh, M. Kondo-Oestreicher, P. Dayer, Drug–drug interactions of new active substances: mibefradil example, Eur. J. Clin. Pharmacol. 55 (1999) 559–565.